Charge Density in the $CoCl_4^{2-}$ Ion: A Comparison with Spin Density and Theoretical Calculations

Brian N. Figgis,* Philip A. Reynolds, and Allan H. White
School of Chemistry, University of Western Australia, Nedlands, W.A. 6009, Australia

The charge density observed by *X*-ray diffraction in Cs_2CoCl_4 is reported by means of maps, multipole refinements, and constrained valence-orbital refinements. A cobalt atom configuration of $3d\text{-}t_2^{3.3(3)}3d\text{-}e^{4.0(4)}4p'^{1.0(3)}$ was obtained with a cobalt charge of +0.7(2) and a chlorine charge of −0.7(1). Within the $CoCl_4^{2-}$ ion the bonding is close to ionic with 0.30(5) e donated from each chlorine atom into, mainly, the diffuse cobalt 4*p*' orbitals. The charge density of the $CoCl_4^{2-}$ ion has a slight trigonal distortion from cubic symmetry whereas the magnetic properties show *mm* symmetry. The difference is rationalised in terms of the arrangement of the chloride ions and of the surrounding caesium ions. This 'intermolecular' effect on the charge density is comparable in size with the covalent redistribution of charge within the ion. Difference density maps and the refinements indicate that close neighbours cause a charge redistribution in the ions from the outermost diffuse orbitals to localised regions at approximately the ionic radius along the interionic vector. This concentration of charge into small regions of space, while an 'intermolecular' effect, is reminiscent of overlap effects often seen in 'true' chemical bonds. In this case the charge transfer of this 'intermolecular polarisation' is comparable in size with those in the Co–Cl bond. The charge density in the $CoCl_4^{2-}$ ion is compared with the experimental spin-density distribution and with theoretical calculations. The qualitative agreement with the theory is good, suggesting that the poor agreement between theory and the spin-density results arises from the neglect of electron correlation effects, to which the spin density is more sensitive, or, less probably, to spin-sensitive effects from the rest of the crystal, as the theory is for isolated $CoCl_4^{2-}$ ions.

X-Ray and polarised neutron diffraction (p.n.d.) experiments, which measure respectively charge- and spin-density distributions, are of sufficient accuracy to provide tests of theories of bonding in transition-metal complexes. An example is the case of $[Ni(NH_3)_4(NO_2)_2]$.[1,2] The experiments show that good quality theoretical wavefunctions obtained by the restricted or unrestricted Hartree–Fock methods are an inadequate description of the results.[3,4] These, or more sophisticated calculations, are much simplified when applied to smaller complexes of high symmetry.

Accordingly, we continue our studies of $MX_4^{-,2-}$ (M = Co^{II} or Fe^{III}, X = Cl[3,5-8] or Br[9]) and MX_6^{3-} (M = Cr^{III}, X = F[10] or CN[11,12]) ions. The $CoCl_4^{2-}$ ion has been much studied theoretically. Recent examples are a Hartree-Fock (HF) calculation including configuration interaction[13] and a discrete variation Xα (DV-Xα) calculation.[14] In a previous paper[4] we compared the spin density in the $CoCl_4^{2-}$ ion, derived from a p.n.d. experiment,[5] with an unrestricted Hartee-Fock (UHF) calculation. While there was qualitative agreement, the covalent transfer of spin was considerably underestimated by the theoretical treatment.

In this paper the results of an *X*-ray diffraction study on Cs_2CoCl_4 at 120 K are presented. They are compared with the theoretical and spin-density results, and with a room-temperature study on Cs_3CoCl_5.[6]

The structure of Cs_2CoCl_4 was determined by *X*-ray diffraction some time ago.[15] The magnetic,[16,17] thermal,[18,19] and optical[20] properties have also been investigated from the melting point (870 K) down to very low temperatures. These studies show no evidence of any phase transition, apart from magnetic ordering at 0.22 K. The $CoCl_4^{2-}$ ion is distorted from an ideal tetrahedron and this is reflected in low-symmetry effects on the spectral and magnetic properties. In our consideration of the relation between the experiments and the calculations on an isolated regular tetrahedral $CoCl_4^{2-}$ ion attention must be paid to these complicating environmental effects.

Table 1. Crystal and experimental conditions for Cs_2CoCl_4

T/K	120(5)
M	1 866.2
Space group	*Pnma*
a/pm	972.0(3)
b/pm	731.3(3)
c/pm	1 282.2(2)
U/nm^3	0.911(1)
Z	4
D_c/kg l^{-1}	3.40
No. of reflections measured	24 093
No. of unique reflections	4 204
$(\sin\theta/\lambda)_{max.}$/nm^{-1}	10.14
λ(Mo-K_α)/pm	71.069
Transmission factors	0.13—0.26
Crystal dimensions/mm (from centre)	(010) 0.1725, ($\bar{1}$01) 0.1200, (101) 0.1500, (111) 0.1125, (1$\bar{1}$1) 0.1175, (11$\bar{1}$) 0.1050, (1$\bar{1}\bar{1}$) 0.1050, (001) 0.1950
F(000)	818.5

Experimental

Deep blue crystals of Cs_2CoCl_4 were grown by evaporation of an aqueous solution of caesium chloride and cobalt(II) chloride hexahydrate. Diffraction data were collected on a cube-like crystal (habit defined in Table 1) using a Syntex $P2_1$ four-circle diffractometer. The crystal was maintained at 120 K by a locally developed cold nitrogen gas flow device. The temperature stability was ±2 K but the absolute temperature was calibrated to only ±5 K. The orthorhombic cell constants were

Table 2. Relative atomic co-ordinates ($\times 10^5$), with e.s.d.s in parentheses (spherical-atom refinement)

Atom	*x*	*y*	*z*
Cs(1)	35 987(3)	25 000	10 074(3)
Cs(2)	2 224(2)	25 000	−17 363(2)
Co(1)	−23 514(5)	25 000	7 772(4)
Cl(1)	− 372(10)	25 000	9 993(9)
Cl(2)	−31 234(11)	25 000	−8 880(7)
Cl(3)	−32 597(9)	50 178(13)	15 283(8)

Table 3. Bond lengths (pm) and angles (°) in the $CoCl_4^{2-}$ ion (spherical-atom refinement)

Co(1)–Cl(1)	226.7(2)	Cl(1)–Co(1)–Cl(2)	116.56(7)
Co(1)–Cl(2)	226.4(2)	Cl(1)–Co(1)–Cl(3)	109.56(4)
Co(1)–Cl(3)	225.8(2)	Cl(2)–Co(1)–Cl(3)	105.82(5)
		Cl(3)–Co(1)–Cl(3′)	109.27(6)

determined by the least-squares fitting of the setting angles of six reflections well spaced in angle. A truncated sphere of data with $2\theta < 75°$ and $h < 11$ was collected, followed by a partial hemisphere with $65 < 2\theta < 95°$, $l > 0$, with experimental conditions as described previously.[1] The crystal and experimental conditions are set out in Table 1. The reflection data were processed with the XTAL data system.[21] After correction for standards, which indicated no detectable crystal decomposition with time, an absorption correction was made using ABSORB of the XTAL system.

Since Cs_2CoCl_4 is a highly absorbing crystal ($\mu = 11$ mm^{-1}) the crystal dimensions were refined by minimising the disagreement between orthorhombic equivalents for 100 low-angle reflections. Pairs of crystal faces were observed to be precisely parallel, so successive changes in the face separations from the mid-point of the crystal while maintaining the crystal volume were made. The agreement factor between equivalent reflections $R_I = \Sigma \text{av.}|I - \text{av.}(I)|/\Sigma \text{av.}(I)$ (av. = average) reduced from 0.093, using the initial optical measurements of the crystal dimensions, to 0.024. The refined dimensions were still within the errors placed on the initial measurements. The refinement procedure gave an apparent accuracy of 0.005 mm in the crystal dimensions. For the complete set of data $R_I = 0.037$ and for the final averaged data $\Sigma\sigma(I)/\Sigma(I) = 0.022$. For the more intense reflections the agreement in orthorhombic equivalents equalled that between Friedel pairs, 0.025, confirming that even in this highly absorbing crystal a correction for absorption sufficiently accurate for charge-density purposes has been achieved.

A thermogravimetric/differential thermal analysis experiment was performed on large crystals of Cs_2CoCl_4 and this confirmed the absence of a phase transition below the melting point.

Refinements.—Three types of refinement of the reflection data were performed: (*a*) traditional spherical-atom refinement, (*b*) conventional multipole refinement, and (*c*) constrained valence-orbital refinement. They are discussed in turn below.

Spherical-atom refinement. Least-squares refinement of atomic co-ordinates, anisotropic thermal parameters, and an isotropic extinction parameter was performed on the data set using the program SFLSX of the XTAL system, in its full-matrix mode. Neutral-atom scattering factors, modified for anomalous dispersion, were used. The function $\Sigma\sigma(F_o)^{-2}(|F_o| - |F_c|)^2$ was minimised for the 2 959 reflections with observed intensity $I_o > 3\sigma(I_o)$. The starting atomic co-ordinates were taken from the earlier structure determination.[15] The final agreement factors were $R(F) = \Sigma(||F_o| - |F_c||)/\Sigma|F_o| = 0.027$ and $R'(F) = \Sigma\sigma(F_o)^{-1}(||F_o| - |F_c||)/\Sigma\sigma(F_o)^{-1}|F_o| = 0.029$. Refinement using only the 1 190 reflections with $\sin\theta/\lambda < 7$ nm^{-1} and $I_o > 3\sigma(I_o)$ gave $R(F) = 0.019$ and $R'(F) = 0.021$.

To provide the less biased estimates of thermal and positional parameters required for the valence-electron analysis, a refinement of the data with $\sin\theta/\lambda > 7$ nm^{-1} and minimising $\Sigma\sigma(I_o)^{-2}(I_o - I_c)^2$ was performed using the local program ASRED.[5] Ionic scattering factors for Co^{2+}, Cs^+, and Cl^- were used[22] as a closer approximation to the valence-electron density. In addition to an extinction correction, an angle-independent intensity was also refined as a crude correction for multiple scattering. These provided a small but significant improvement in the goodness-of-fit, χ. The 2 808 data with 41 variables gave $R(I) = \Sigma|I_o - I_c|/\Sigma I_o = 0.066$, $R'(I) = \Sigma\sigma(I_o)^{-1}(I_o - I_c)/\Sigma\sigma(I_o)^{-1}I_o = 0.080$, and $\chi = 0.820$. A test refinement using Type II uniaxial anisotropic extinction was made, which showed that the extinction was isotropic within an error of 3% in the extinction correction factor. The positional parameters are given in Table 2. Bond distances and angles are given for the $CoCl_4^{2-}$ ion in Table 3. A similar refinement with $\sin\theta/\lambda < 7$ nm^{-1} gave $R(I) = 0.0265$, $R'(I) = 0.0422$, and $\chi = 1.023$ for 1 396 reflections. The scale factor for this refinement increased from the high-angle result by only 1.2%, while the diagonal elements of the thermal motion tensor decreased by an average of 4.6%. Given the low thermal motion at 120 K, $\langle U \rangle^2 \sim 200$ pm^2, errors caused by inaccurate positional and thermal parameters will be negligible for valence-electron refinement purposes.

A rigid-body analysis of the thermal motion of the $CoCl_4^{2-}$ unit was performed.[23] The 12 independent thermal libration screw-displacement (*TLS*) elements together with the 18 independent thermal parameters of the $CoCl_4^{2-}$ unit gave $R(I) = 0.038$. If only the eight *TL* elements were employed $R(I) = 0.15$. Both the *T* and *L* matrices were almost diagonal; $T_{11} = T_{22} = 0.9$, $T_{33} = 1.4$ nm^{-2}, $L_{11} = 4.6$, $L_{22} = 16.7$, $L_{33} = 6.9°^2$. However, the poor observation-to-parameter ratio prevents any interpretation other than that these numbers are a recasting of the thermal motion tensor into a more comprehensible form. We do not suggest that the $CoCl_4^{2-}$ ion is more rigid than the rest of the lattice.

In order to provide a benchmark for the valence-electron refinements, a refinement of all the data varying only the scale factor and the extinction parameter while using the high-angle positional and thermal parameters with Cs^+, Co^{2+}, and Cl^- scattering curves was performed (R1). We obtained $R(I) = 0.0284$, $R'(I) = 0.0437$, and $\chi = 1.0399$. Deformation density maps based upon this 'promolecule' are shown in Figure 1 for the plane ($y = \frac{1}{4}$) containing all the atoms but Cl(3).

Multipole refinement. Using the values of the positional and thermal parameters from the high-angle spherical-atom refinement we performed a multipole refinement of the valence-shell electrons using all 1 396 data with $\sin\theta/\lambda < 7$ nm^{-1} (R2). We expected 3*d*-like populations on the cobalt and 3*sp*-hybrid-like populations on the chlorine atoms. Thus all crystallographically-allowed multipoles up to order 2 on caesium and chlorine atoms were refined. On caesium a 1*s* form factor with $\xi = 1.2$ a.u.$^{-1}$ (*ca.* 2.3×10^{-10} m^{-1}) was initially employed to allow polarisation of these large ions. On chlorine the form factors of atomic chlorine 3*p* radial density were used. On cobalt we used atomic 3*d* form factors with all multipoles of order up to 4, and in addition a 4*p* atomic radial function with all multipoles up to order 4. This 4*p* function is very diffuse and extends over much of the $CoCl_4^{2-}$ ion. Where not tabulated the required angular scattering functions $\langle j_m \rangle$[22] were calculated

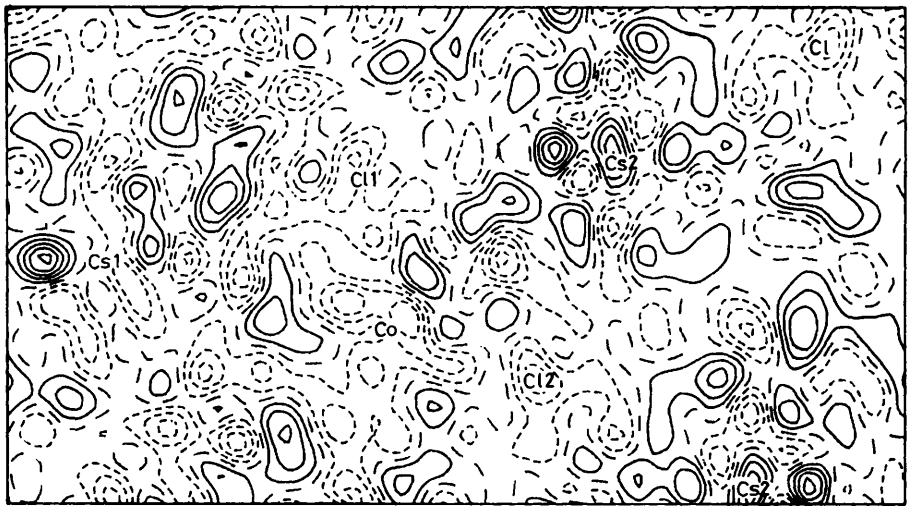

Figure 1. Deformation charge-density map for the $y = \frac{1}{4}$ plane in Cs_2CoCl_4. The contour interval is 200 e nm^{-3}, solid lines positive, dashed negative. The plane extends from $(0,\frac{1}{4},0)$ at the bottom left to $(\frac{1}{4},\frac{1}{4},1)$ at the top right. The positions of Cs(1), Cs(2), Co(1), Cl(1), and Cl(2) are marked

from the atomic wavefunctions of Clementi and Roetti[24] using a local program JCALC.

Using the crystallographic point symmetry, with z parallel to c and x parallel to a, the multipole set consisted of 54 functions. To provide further flexibility, the extents of the cobalt 3*d*-like and the chlorine 3*p*-like form factors were allowed to vary by calculating the scattering at $K_{nl}\bar{s}\cdot\bar{r}$ rather than at $\bar{s}\cdot\bar{r}$ ($\bar{s}$ is the scattering vector and K_{nl} a parameter associated with the *nl* form factor *l*). Thus, together with the scale factor and an isotropic extinction parameter, a total of 60 variables were involved. The total electron population was constrained at the formula value.

Since the caesium scattering is so large, refinement was also performed where the caesium site occupancy was allowed to vary. This has the effect of optimising the Cs^+ form factors against the contribution from the $CoCl_4^{2-}$ ion, and of allowing for possible contamination of the caesium by lighter alkali metals. This final model contained 62 variables. With the 1 396 data we obtained (R2) $R(I) = 0.0229$, $R'(I) = 0.0370$, and $\chi = 0.895$, a significant improvement on the spherical-atom refinement, R1.

At the 3σ level many of the higher-order multipoles (*i.e.* above Y_0^0) were not of significant magnitude. The only ones significant at that level were Y_2^2 on Cs(1), Y_1^1, Y_2^0, and Y_2^2 on Cs(2), Y_1^1 and Y_2^{-2} on Cl(3), and Y_1^1, Y_2^{-2}, and Y_4^{-2} for the 4*p* set on Co(1). In particular, *no* higher order multiples on Cl(1) or Cl(2) or in the Co(1)-3*d* set met the criterion.

It is evident from the residual charge-density map obtained from the results of this refinement that the major remaining source of discrepancy lies in the caesium atom regions. Accordingly, the number of basis functions on Cs(1) and Cs(2) was increased. Guided by the residual density, 5*p* and 4*d* functions calculated for xenon[24] were used. Such functions change but little between Xe, I, Xe^+, and I^+, and thus provide a reasonable approximation for Cs^+. For *each* radial function all crystallographically-allowed multipole functions up to order 4 were permitted to minimise, a total of 30 functions for each Cs atom. In addition, the caesium atom populations and 4*d* and 5*d* radii were allowed to refine. This refinement, R3, of 112 variables, gave $R(I) = 0.0209$, $R'(I) = 0.0341$, with $\chi = 0.820$.

The major part of the improvement arises from Y_4^0 and Y_4^4 in the 4*d* radial set. Their ratio indicates an almost cubic symmetry. The remainder of the higher-order multipoles are not large and so do little to improve either the fit or the residual density maps. In particular, the series of peaks at *ca.* 150 pm from each Cs atom are not markedly reduced in height. Even such an extensive angularly and radially flexible set cannot model these localised functions well.

The zeroth-order multipoles (Y_0^0), representing overall atom populations, are of interest, with Cl(1) < Cl(2) ~ Cl(3). However, the Cs(5*p*), Co(4*p*), and Cl(3*p*) functions are very diffuse with scattering decreasing rapidly when $\sin\theta/\lambda$ exceeds 2—3 nm^{-1}, and the associated parameters are being fitted to less than 50 observations. Given that extinction affects intensities in this region of reciprocal space by up to 30%, there is likely to be an over-parameterisation of the data. Consequently, although the interatomic correlation coefficients are small, the difference in Cl populations cannot be regarded as of much significance. To test the reality of such population differences requires a substantial reduction in the number of parameters to be varied.

The observation that the cubic '4*d*' distortions from spherical symmetry on the caesium atoms have the same axis system prompts a suspicion that errors in absorption or extinction corrections are responsible. We therefore performed two further refinements in which absorption and extinction parameters corresponding to cubic symmetry were allowed to vary. Neither change was found to be significant, so that the effect probably does not arise from inadequate corrections to the experimental data. The higher-angle data, more dominated by the caesium atom cores, does not show this cubic symmetry. Thus anisotropic anharmonic motion of the conventional type, which varies as $(\sin\theta/\lambda)^4$, is not likely to be a cause of the effect, either.

In conclusion we can probably approach the goodness-of-fit of this full-scale multipole model by the use of a more efficient model, with fewer variables, in which constraints amongst the atoms are introduced, perhaps including cubic symmetry in the $CoCl_4^{2-}$ ion. This possibility is examined in the following 'constrained valence-orbital' refinement section.

Constrained valence-orbital refinements. Since our interest focuses on the $CoCl_4^{2-}$ ion, in this valence refinement, we simplify the fitting for Cs(1) and Cs(2), guided by the multipole refinement results.

On each caesium atom we refine a '4*d*' and a '5*s* + *p*' (the 5*s* and 5*p* form factors are very similar) spherical population and a 4'*d*' term of cubic symmetry, whose axes lie along *a* and at 45° to *b* and *c*. In addition, guided by the residual density map, we

have refined a term, p_{shell}, corresponding to a thin spherical shell of electron density at radius, r_{shell}, from each caesium atom. This shell has the form factor $f_{shell}\vec{s} = p_{shell}\cdot\sin(2\pi|\vec{s}|r_{shell})/(2\pi|\vec{s}|r_{shell})$. Both populations and radial parameter were refined.

The charge density on the $CoCl_4^{2-}$ ion is constrained to be cubic in symmetry. On Co(1) we refine $3d$-t_2, $3d$-e, diffuse '$4p$' functions, and a shell population with r_{shell} = 150 pm. The radial extent of the $3d$ functions is allowed to vary as described in the multipole refinement section. The three crystallographically independent chlorine populations are constrained to be equal. Thus there are four chlorine atom populations; sp_1 (directed at the cobalt atom), sp_2 (180° to sp_1), and $3p_\pi$, all with a common radial expansion parameter, and p_{shell} (with r_{shell} fixed at 150 pm). Compared with the final multipole refinement, the number of variables is reduced from 112 to 22. This refinement (R4) gave $R(I)$ = 0.0241, $R'(I)$ = 0.0366, and χ = 0.8730.

Table 4. Results of valence-electron refinement R4

Atom	Parameter	Value
Cs(1)	'$4d$'	9.6(3)
	'$5s + p$'	7.2(4)
	p_{cubic}	8.1(6)
	p_{shell}	1.6(2)
	r_{shell} (pm)	1.45(7)
	total charge	+0.6(2)
Cs(2)	'$4d$'	9.9(2)
	'$5s + p$'	7.0(6)
	p_{cubic}	8.1(5)
	p_{shell}	0.6(2)
	r_{shell} (pm)	1.6(1)
	total charge	+1.6(2)
Co(1)	$3d$-t_2	3.3(3)
	$3d$-e	4.0(3)
	'$4s + p$'	1.2(3)
	p_{shell}	−0.2(3)
	K_{3d}	1.05(3)
	total charge	0.7(2)
Cl	$3(sp)_1$	1.93(8)
	$3(sp)_2$	1.86(8)
	$3p_\pi$	3.40(15)
	p_{shell}	0.5(1)
	K_{3p}	0.97(1)
	total charge	−0.7(1)

In this refinement the core populations, except for Cs $4d$ and $5p$, were not refined and the total number of electrons was not constrained to the formula value. We thus have two indicators of the adequacy of the modelling: the ratio of the scale factor of R4 to that of the high-angle valence refinement, 1.0050, and the estimated value of $F(000)$, 823.8 e, compared with the formula number, 818.5. The agreements are excellent. We note the removal of the 'shell' parameter changes the scale factor ratio to 1.020 and $F(000)$ to 840, and worsens the fit. The residual results are given in Table 4. The residual maps are little altered from the deformation density maps and so are not shown. The refinement is much closer to the full multipole results, *viz.* χ = 0.87 *versus* 0.82, than the spherical-atom case, χ = 1.04. This confirms our earlier conclusion that the extensive 30 parameter per Cs multipole model still cannot fit the remaining density.

The effect of constraining the $CoCl_4^{2-}$ ion to cubic symmetry may be investigated by relaxing the symmetry to *mm* or to $3m$. The $CoCl_4^{2-}$ fragment possesses only a mirror plane of crystallographic symmetry. As noted by Porai-Koshits,[15] the 11 nearest-neighbour caesium atoms are disposed with almost *mm* symmetry. That symmetry also conforms with the magnetic anisotropy results.[25] An alternative description of the atomic arrangement is that the cell is almost hexagonal, being only 8% distorted from a hexagonal close-packed arrangement of the cobalt atoms. Indeed, the isomorphous salt α-K_2SO_4 shows a phase transition to the $P6_3/mmc$ (β-K_2SO_4) form by disordering of the SO_4^{2-} ions to give a centre of symmetry, together with some *small* atomic positional shifts.[26]

The goodness-of-fit is not significantly improved in refinements using these symmetries, and the parameter values change but little. The only exception is that in $3m$ symmetry the chlorine populations differ at the 2σ significance level: Cl(1), 7.3(3) e; Cl(2) = Cl(3), 7.9(3) e. The refinement results are summarised as follows.

1. A simple valence refinement for the $CoCl_4^{2-}$ ion, assuming cubic symmetry and using $3d$ and $4s$ orbitals on Co and $3s$–$3p$ hybrid orbitals on Cl, produces a significant improvement on the spherical-atom refinement R1.
2. Allowing the Cs atoms to adopt cubic symmetry produces a significant improvement in the fit.
3. A term corresponding to a thin shell of electron density at a radius of 150 pm from each Cs atom is also significant.
4. The resulting residual density cannot be fully fitted by an extensive multipole model (R3).

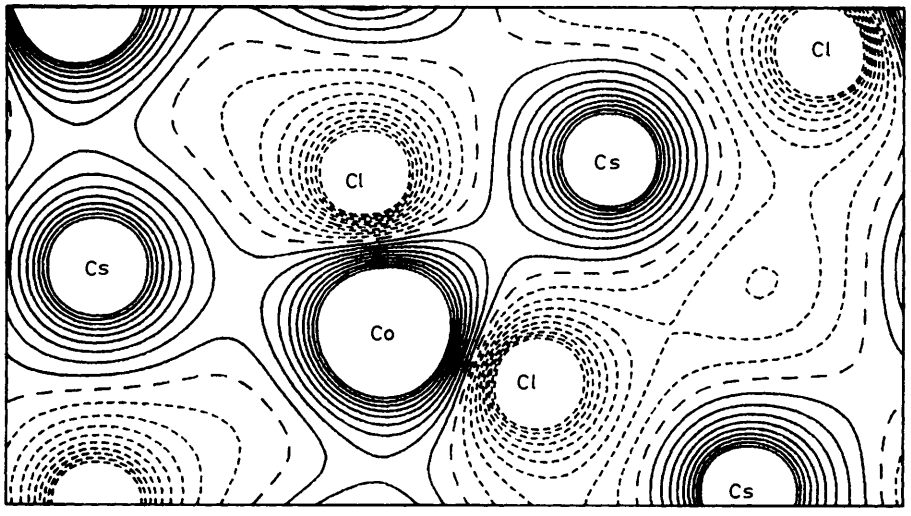

Figure 2. The calculated electrical potential in the $y = \frac{1}{4}$ plane of Cs_2CoCl_4, as in Figure 1. The contour interval is 100 e nm^{-1}

Table 5. The correlation between deformation density and short interatomic vectors. *All* vectors in the $y = \frac{1}{4}$ plane (except Co–Cl bonds) of <600 pm are listed. *All* deformation density peaks are also listed

Interatomic vector		Interatomic distances	Peak–M(1) distances	Peak crystal co-ordinates ($\times 10^3$)	
M(1)	M(2)	(pm)	(pm)	*x*	*z*
Co(1)	Cs(1)	394.7	160	276	293
Co(1)	Cs(2)	407.9	100	350	460
Co(1)	Cs(1)	422.6	130	654	21
Co(1)	Cs(2)	569.3			
Cs(2)	Cl(2)	342.8	120	417	628
Cs(2)	Cl(2)	344.5	160	541	795
Cs(2)	Cl(1)	351.6	170	457	556
Cs(1)	Cl(1)	353.4	200	462	238
Cs(1)	Cl(2)	400.6	180	536	59
Cs(1)	Cl(1)	406.1	200	164	67
Cs(1)	Cs(2)	481.1	280	271	887
Cs(1)	Cs(1)	524.0	260	615	192
Cs(2)	Cs(2)	524.0	170	694	707
Cs(2)	Cs(1)	569.8	270	468	887
Cs(2)	Cs(1)	481.1	130	592	632
Cs(1)	Cs(1)	524.0			
Cs(2)	Cs(2)	524.0	150	417	711
Cs(1)	Cs(2)	481.1	310	468	887

Electrical Potential Calculations.—Figure 2 shows the electrical potential in the *xy* plane at $y = \frac{1}{4}$, calculated using a point-charge model and a locally modified version of the program MADLUNG.[27] Four further plots were made of the potential on removal of respectively the $CoCl_4^{2-}$, Cs(1), Cs(2), and Co(1) fragments, but are not shown.

Results and Discussion

The structure of Cs_2CoCl_4 has been fully discussed elsewhere.[15] The higher precision here produces no changes worthy of comment.

Deformation Density Maps.—The deformation density maps in Figure 1 contain a large number of peaks, at first sight randomly distributed! Close to each caesium atom, at a distance of *ca.* 70 pm, we see two peaks along *a* and four peaks out of the plane corresponding to cubic symmetry and which we have fitted with the cubic '4*d*' population. The rest of the map can be regarded as being composed of peaks superimposed upon a relatively smooth negative background. There are 15 such peaks in the $y = \frac{1}{4}$ plane which have an electron density exceeding 400 e nm^{-3}. *All* of them lie between 100 and 200 pm from a metal ion and near a short interatomic vector. The angular deviation of the peaks from the metal–neighbour vector averages only 10°, with a maximum of 30°. Moreover, if the atomic vectors are classified by type and length, *all* the Cs–Cs, Cs–Cl, and Cs–Co vectors less than 600 pm have an associated peak, except for the two longest Cs–Cs and Co–Cs separations (see Table 5). Such an excellent correlation provides a qualitative explanation of the features in this complicated difference density. Each short Co–Cs vector contains a peak at 130(30) pm from the cobalt atom, each Cs–Cl vector contains a peak 170(30) pm from the Cs atom and 180(30) pm from the Cl atom, and each Cs–Cs vector contains *two* peaks, one 220(7) pm from each Cs atom. By noting that the ionic radii of Cl^-, Cs^+, and Co^+ are 180, 170, and 130 pm respectively, the deformation density can be explained in the following way. When the ions are assembled to form the crystal, diffuse electron density is rearranged by concentrating it into regions of higher density along each short interionic vector at a distance corresponding to the edge of the normal free-ion electron density. Such a situation is reminiscent of the mostly larger effects of the same type occurring in the formation of much shorter recognisably chemical bonds.

Valence-orbital Refinements.—(*a*) *Caesium atoms.* The caesium atom form factors deviate only slightly from the theoretical curves, but the differences are important for fitting the present data. Given the high atomic number, the quality of the atomic wavefunctions for caesium, and hence of the calculated form factors, is expected to be limited to say 2%, which is nearly the size of the observed deviations. Also, anharmonic and crystal-field polarisations could alter the effective shape of the form factors. We remark that (*i*) the form factors for the two caesium sites are very similar and differ significantly, if only slightly, from free-atom curves, and (*ii*) the correlation between the Cs-based variables and those of the $CoCl_4^{2-}$ ion is low (correlation coefficients <0.15) so that errors in the treatment of the former will have little effect on the latter.

The mean caesium charge, +1.1(5), shows that little charge transfer involving the Cs^+ ion has taken place. There has however been a shift of *ca.* 1 e from the '5*s* + *p*' orbitals into a more constricted region which has been modelled by a thin spherical shell of radius 150 pm. This result is consistent with the qualitative interpretation of the difference density where we observe the peaks along short interionic vectors at these distances. The refinement indicates that these peaks are derived by a rearrangement of the most diffuse '5*s* + *p*' caesium orbitals.

The Cs(1) and Cs(2) charges differ by 5σ (1.0 e) from each other. This large difference may be a reflection of the poor fit to the individual caesium form factors which were discussed earlier. The complex angular and radial rearrangements revealed in the deformation density maps and suggested by the large values of the parameters, p_{shell}, p_{cubic}, and '5*s* + *p*' are not well fitted even by the extensive multipole model R3, and differ between Cs(1) and Cs(2). Thus the difference in apparent Cs(1) and Cs(2) charges reflects the inadequacy of the model in the Cs region in describing the intermolecular effects, which differ between the two atoms.

We note that not only do the low correlation coefficients between the caesium atoms and the $CoCl_4^{2-}$ ion region enable us to discuss that ion with more precision than the caesium atoms, but also in this centrosymmetric structure the phases are fixed at ±1 and therefore are markedly insensitive to details around those atoms. Thus the deformation density maps are also little affected by deficiencies in our simple caesium form-factor modelling.

The anisotropy in the '4*d*' distribution seems too large to be a radial polarisation effect. It is not likely to be an experimental artefact since the core electrons do not participate, as is shown by the $\bar{s}$ dependence. This may indicate that the '4*d*' + '5*s* + *p*' thermal motion may not follow the core exactly and is also anharmonic. If we allow for a non-rigid caesium ion and apply a shell model of the motion we would expect the core motion to be more harmonic than that of these valence electrons. Our evidence is too tenuous to make that conclusion more than suggestive.

A counter argument, that it is not a motional effect but a polarisation of the static charge density, could be based upon the fact that calculations suggest that the caesium ion has very high electric hyperpolarisabilities. Both the octupolar[28] and hexadecupolar[29] polarisabilities are three times greater than Rb^+, ten times greater than K^+, and hundreds of times larger than Na^+. Given that the Cl^- ion also has a very large hyperpolarisability,[30] perhaps the observation of substantial high multipole-order polarisations is not unreasonable.

Table 6. (*a*) Valence-electron charges in the $CoCl_4^{2-}$ ion, cubic symmetry assumed, shell populations distributed. (*b*) Valence-electron spin populations for $CoCl_4^{2-}$

		(*a*)			(*b*)		
		X-Ray (exptl.)	UHF (calc.)	DV-Xα (calc.)	p.n.d. (exptl.)	UHF (calc.)	DV-Xα (calc.)
Co	$3d$–t_2	3.3(3)	3.14	3.20	2.86(3)	2.90	2.75
	$3d$–e	4.0(3)	4.01	4.00	−0.22(3)	0.00	0.00
	'4*s*'	1.0(3)	0.33	1.13	0.06(5)	0.01	0.14
	K_{3d}	1.05(3)			0.961(5)		
	Net charge/spin	+0.7(2)	+1.53	+0.67	2.70(4)	2.91	2.89
Cl	$3(sp)_1$	2.1(1)	3.88	3.66	0.024(9)	0.02	0.03
	$3(sp)_2$	2.0(1)			0.035(5)		
	$3p_\pi$	3.7(1)	4.0	4.0	0.019(8)	0.00	0.00
	K_{3p}	0.97(1)					
	Net charge/spin	−0.7(1)	−0.88	−0.67	0.08(1)	0.02	0.03

(*b*) *The* $CoCl_4^{2-}$ *ion.* The observed charge distribution in the $CoCl_4^{2-}$ ion, set out in Table 6, agrees as well as might be expected with that found in a more limited analysis, in Cs_3CoCl_5.[6] There the observed cobalt atom configuration of $3d^{7.1(1)}4p'^{0.6(2)}$ gave net charges of +1.3(1) on cobalt and −0.8(1) on chlorine.

A valence refinement using the model of R4 on the data for Cs_3CoCl_5 (295 K) gave results consistent with the present treatment. However, the errors, particularly in non-spherical features such as t_2/e populations, were too large to make those features significant. The errors arose principally because the high thermal motion greatly reduced the intensity of data with $\sin\theta/\lambda > \sim 5$ nm^{-1}. Since information in that region is necessary to analyse the non-spherical features, these latter become ill defined. In addition there was noticeable anharmonicity in these data precluding use of the highest-angle members ($\sin\theta/\lambda > 7$ nm^{-1}). This illustrates the point that the information gained by the use of low temperatures is critical for valence-electron distribution studies.

The $CoCl_4^{2-}$ unit thus seems quite close to an assembly of free prepared ions. That is the $3d$ configuration on cobalt from the present study, $t_2^{3.3(3)}e^{4.0(4)}$, is not significantly different from the ionic crystal-field model configuration $t_2^3e^4$. The chlorine configuration is scarcely different from spherical. We conclude that our observations differ from a crystal-field model mainly in that 1.3(2) electrons have migrated from the four chloride ions into diffuse cobalt-based orbitals, which we have labelled '4*p*'. The '4*p*' orbitals are actually *so* diffuse that they envelop the chlorine atoms, so the distinction between Co and Cl is rather artificial. The contraction of the chlorine $3p$ radial parameter by 3(1)% is consistent with the charge migration: as the chlorine charge increases from −1 towards 0 we expect a gradual contraction from a Cl^- to a Cl^0 form factor. Chemical experience would lead us to expect σ-bonding to dominate π-bonding, with a consequent increase in the Co t_2 population, a decrease in Cl $(sp)_1$ and perhaps in $(sp)_2$ also, with little change in Co e and p_π populations. Although scarcely at the level of significance, our data suggest the converse. On the cobalt atom this may be an artefact of the modelling. Part of the diffuse density which we have modelled as '4*p*' could just as well be labelled 4*d*. A refinement using diffuse *d* functions[31] gives a very similar fit to the data with ~0.75 e in them, and a cobalt configuration of $t_2^{3.5(3)}e^{4.0(4)}$. On the chlorine atoms the partitioning of charge between σ and π depends on the assumption of a common radial dependence.

In a study on the $FeCl_4^-$ ion[8] we observed strong polarisation of the chlorine atoms which we attributed to 'intermolecular' effects. The observed trigonal distortion in the $CoCl_4^{2-}$ ion charge density seems to indicate that intermolecular effects are of about the same size as charge transfers within the $CoCl_4^{2-}$ ion due to covalence. A further indication of this is the size of the 'shell' populations (Table 4). Their magnitude is comparable with the charge transfer within the $CoCl_4^{2-}$ ion, and we have attributed their origin to the influence of 'non-bonded' nearest-neighbour ions.

As we have seen, at the cobalt atom the $CoCl_4^{2-}$ ion local symmetry can be described in terms of *mm* or trigonal symmetry depending on the factors which are considered to be important. Again, the immediate environment of the caesium atoms is closer to *mm*, but at larger distances it becomes trigonal. The chlorine atom environments were examined in more detail. Each chlorine atom is surrounded by an approximate trigonal bipyramid of other atom nearest neighbours, *viz.* four caesium atoms with the cobalt atom at one 'axial' position. The four caesium atoms comprise one 'axial' and three 'equatorial'. The equatorial caesium atoms are each nearest neighbours to two chlorine atoms in the $CoCl_4^{2-}$ units, so each such unit has 10 Cs^+ nearest neighbours. For Cl(1) the mean Cs–Cl distances (365.3 pm) are noticeably longer than in the cases of Cl(2) and Cl(3) (356.3 and 357.3 pm). The observed extra diffuseness of the charge density around Cl(1) compared to Cl(2) and Cl(3) is thus mirrored by the larger hole that it inhabits. Whether that is the *cause* can only be determined by further theoretical calculations, particularly of the magnitudes of Cl nearest-neighbour and long-range effects, which are both of trigonal symmetry.

The point-charge electrical potential calculations, of which Figure 2 presents an example, do, however, show that the potential gradient at any ionic site is dominated by nearest-neighbour effects. More distant neighbours together produce a relatively uniform potential over a given ionic site. A point-charge model should be a realistic approximation for such long-range electrostatic effects, even if not for the nearest-neighbour contributions. This calculation supports our interpretation of the trigonality of the $CoCl_4^{2-}$ ion environment and the polarisation of the ions observed in the difference maps as being of *short-range* origin.

The magnetic properties of Cs_2CoCl_4 are best explained by the use of *mm* symmetry. The $CoCl_4^{2-}$ ion itself is almost uniaxial with the relevant axis being through Co(1) and bisecting Cl(1) and Cl(2).[25] Inspection of the bond lengths and angles in Table 3 suggests that the *mm* symmetry [Cl(1) = Cl(2) ≠ Cl(3)] is a better description of the immediate cobalt environment than is trigonal symmetry [Cl(1) ≠ Cl(2) = Cl(3)]. The bond length differences are small, the major influence being the Cl(1)–Co(1)–Cl(2) angle which differs from the ideal tetrahedral value (109.5°), causing a tetragonal distortion. The resulting magnetic anisotropy conforms to that

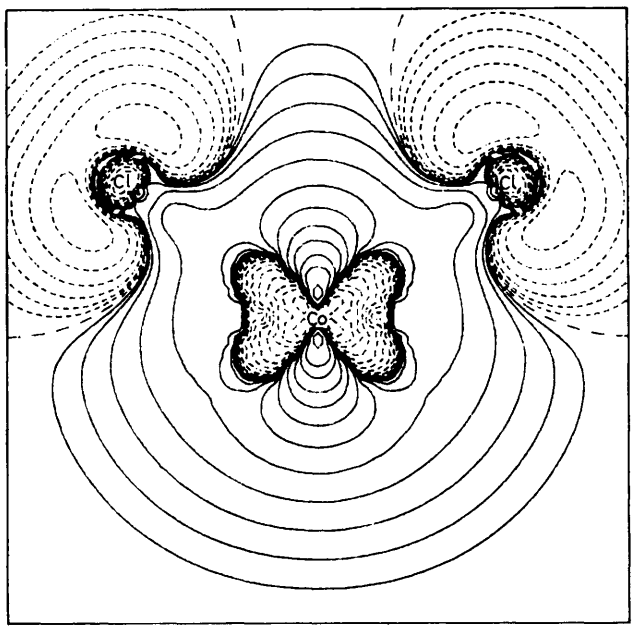

Figure 3. The model deformation charge density in the $CoCl_4^{2-}$ unit in Cs_2CoCl_4. A $CoCl_2$ section is shown with the $\bar{4}$ axis vertical. Spherical Co^{2+} and Cl^- ions have been subtracted. Contours are in geometrical progression with a factor of two between each. The first solid line is at 1.64 e nm^{-3}. Dashed lines represent negative density

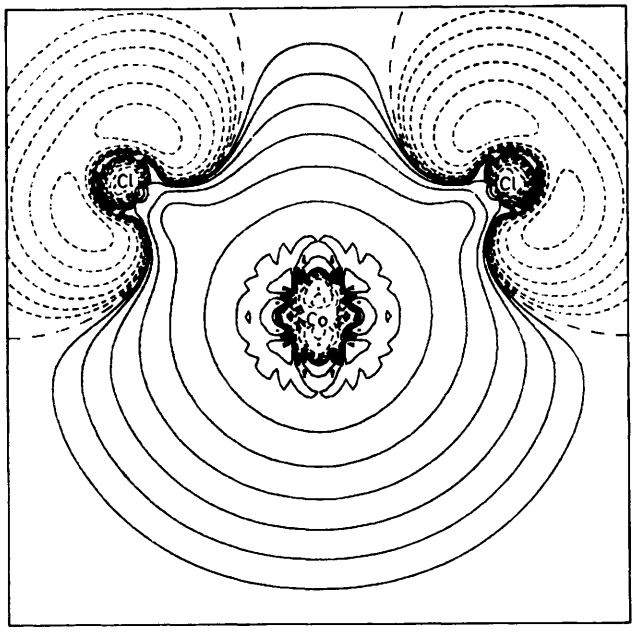

Figure 4. The model residual charge density in the $CoCl_4^{2-}$ unit. Spherical Cl^- and cubic ($t_2^3e^4$) Co^{2+} ions have been subtracted. Contouring is as in Figure 3

symmetry.[16,17] These anisotropies mostly support the idea of the primary influence of the nearest-neighbour ligands.

The difference between the magnetic axis and that of the charge-density distribution is therefore a reflection of the *trigonal* symmetry of the Cl–Cs contacts and further neighbours which is reflected in the trigonal symmetry of the Cl^- and Co-centred diffuse density. On the other hand, the magnetisation density, and equivalent spin density,[2,3] are mainly specially restricted to the Co t_2 orbitals, and so the magnetism reflects the local symmetry of the Co–Cl contacts, which we have seen are of *mm* symmetry.

Comparison with Spin Density.—The spin-density results[3,5] on $CoCl_4^{2-}$ given in Table 6(*b*) are from the compound Cs_3CoCl_5, where the environment is of tetragonal symmetry. Qualitatively, the results are much as expected,[3] with the spin mainly in $3d$–t_2 orbitals on cobalt, with some delocalised mainly by σ bonding onto the chlorine atoms.

As noted in other systems[1,2,7,8] the spin density gives much more precise information on covalency than does the charge density. This is mainly because the spin resides essentially in the valence orbitals whereas the charge density includes all the core electrons, and these tend to dominate the *X*-ray diffraction process. Again, as far as the separation of σ- and π-bonding is concerned, small differences in the radial extent of orbitals have little effect on the modelling of spin density, but are quite critical for the charge densities.

An interesting aspect is that theoretical studies show that electron correlation effects on charge densities may not be appreciable relative to experimental uncertainties, whereas they are quite important for spin-density distributions. A configuration interaction calculation from a Hartree-Fock wavefunction for the $CoCl_4^{2-}$ ion reveals little change in the charge density.[13] On the other hand, the spin density shows appreciable regions of negative spin, which can only arise from correlation effects.[3] Thus, while spin density results are a more stringent test of valence region wavefunctions, they are much more difficult to compare in depth with theory than are charge densities.

If the spin and charge densities are compared using only the qualitative expectations of l.c.a.o.–m.o. (linear combination of atomic orbitals and molecular orbital) theories, interesting features are observed, apart from the encouraging general agreement. The $3d$ radial parameter in the charge case, 1.05(3), corresponds to a noticeably more expanded distribution than in the spin case, 0.961(5). There may be two reasons for the smaller radius for spin.

First, electron correlation spin-polarises filled, formally spin-paired, orbitals giving additional positive spin closer to the cobalt nucleus. This spin polarisation will hardly be noticeable in the total electron populations which constitute the charge density.

Secondly, the spin resides in $3d$–t_2 orbitals ($\sim t_2^3$) while the charge is more in the e orbitals ($\sim t_2^3e^4$). On purely electrostatic arguments a larger size has been predicted for the e (non-bonding) orbitals than for the t_2 (bonding) orbitals.[32] This 'differential nephelauxetic effect' cannot be tested with our *X*-ray diffraction data alone because it would be highly correlated with other variables, particularly the difference between the t_2 and e populations. Another interesting feature is the large cobalt-centred diffuse component of the charge density, whereas there is none of significance in the spin case. This difference in the '$4p$' involvement in bonding and antibonding orbitals is not expected using simple theories, although it has been observed previously.[3,5,7,8]

Charge and Spin Density Maps.—It can be difficult to comprehend the deformation charge- and spin-density maps. Accordingly Figures 3—6 depict different aspects of the experimental results. There the densities have been averaged to tetrahedral, $T_d(\bar{4})$, symmetry. These maps are exact representations of the fitted-model results, and so certain features are fixed by the assumptions inherent in the model, for example the complex nodal behaviour near the nuclei. However, the important larger scale features are determined by the

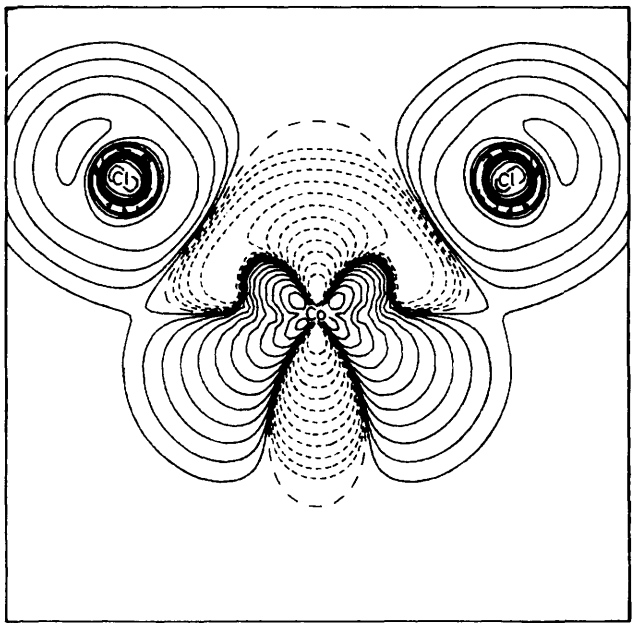

Figure 5. The model deformation spin density in the $CoCl_4^{2-}$ unit. A spherical Co^{2+} ion ($t_2^{1.8}e^{1.2}$) has been subtracted. Contouring is as in Figure 3 except that the first line is at 1.64 spins nm^{-3}

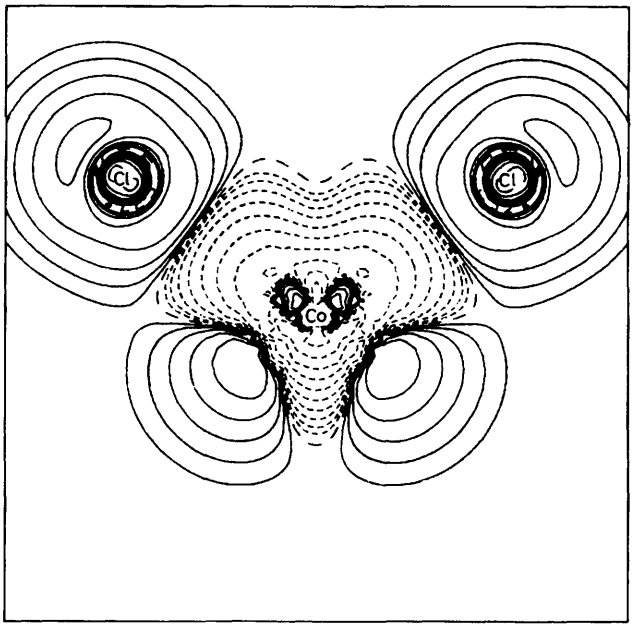

Figure 6. The model residual spin density in the $CoCl_4^{2-}$ unit. A prepared cubic Co^{2+} ion ($t_2^3e^0$) has been subtracted. Contouring is as in Figure 5

experiment. Being representatives of the *total* charge or spin, within the limitations above, these are suitable for direct comparison with theoretical calculations, thus avoiding the process of breakdown into atomic populations.

Figure 3 shows two major features, the rearrangement of 3*d* charge density away from t_2 into the *e* orbitals, and the large diffuse population around the metal atom. The polarisation of the chlorine atom, shifting charge into the Co–Cl bond region, although barely significant, is in the direction expected from simple bonding theory. The π depletion seems greater than σ, and this may reflect intermolecular effects from neighbouring caesium ions. In Figure 4, a prepared $t_2^3e^4$ cobalt atom, rather than a spherical one, has been subtracted. It shows that the cobalt 3*d* region has a density almost identical to a free $t_2^3e^4$ Co^{2+} ion. The complex structure and deep hole near the nucleus reflects a small radial change in the model 3*d* orbitals.

For comparison, Figures 5 and 6 show experimental model deformation and residual spin densities. The difference is striking, and qualitatively as we might predict on simple grounds. Figure 5 shows the concentration of spin in t_2 and depletion in *e* orbitals expected for an approximately $t_2^3e^{0-}$ spin configuration. The covalence, giving spin on the chlorine atoms is also obvious. In Figure 6 we have removed from the total spin density a prepared $t_2^3e^0$ Co^{2+} ion with radial dependence given by theory. From this Figure, the cobalt configuration differs somewhat from a prepared $t_2^3e^0$ ion. In particular, on the cobalt atom there is a polarisation of the spin away from the bond region to areas farthest from all the chlorine atoms in the three-fold axis. There is also a suggestion of a similar polarisation of chlorine atom density away from the bond.

Comparison with Theoretical Work.—While the interesting *mm* and trigonal symmetry effects can only be quantitatively explored by further suitable theoretical work, our results have much bearing on existing calculations on the $CoCl_4^{2-}$ ion in T_d symmetry. At first glance the UHF and DV-$\chi\alpha$ calculations on the ion [Table 6(*b*)] are noticeably different. However, Mullikan populations are notoriously sensitive to changes in basis sets, so the differences may be illusory.

Both these calculations, like the *X*-ray and p.n.d. experimental results, can be *broadly* rationalised in terms of a l.c.a.o.–m.o. treatment of the bonding, *viz.* Co $t_2^3e^4$ with some σ bonding from the chlorine atoms. However, in detail, and at a level relevant to the experiments, there are differences. For example, the simple theories predict that, if the charge in the 3*d*–t_2 orbitals is $3 + \Delta$ then the spin is $3 - \Delta$. Higher level calculations show that this is untrue, and the discrepancy is at a level greater than the experimental uncertainty arising from the p.n.d. experiment. Thus simultaneous refinement of p.n.d. and *X*-ray data with constraints on the parameters between the experiments is invalid at the simple level. Spin and charge densities are separate observables whose connection is complex. Even the discussion of nephelauxetic and correlation effects on 3*d* orbital radii is undoubtedly oversimplified. Although an approach to the simultaneous analysis of *X*-ray and p.n.d. data has been developed,[33] the quantitative comparison of spin and charge densities at this stage seems best made by relating each to a suitable theoretical calculation. Such calculations, in addition to the expected σ-bonding effects, do show a substantial '4*s* + *p*' component in the charge density, and a negligible such component in the spin density, a result which has not been rationalised in simpler treatments.

The earlier comparisons of spin densities and theory noted that the 'covalence', *i.e.* the spin population on the chlorines in simpler models, is considerably underestimated by the calculations, perhaps by a factor of four. From the present charge-density results we can see that the theoretical *charge* transfers are *not* underestimated by such a large factor. This is probably the major conclusion of the present study. In the $CoCl_4^{2-}$ ion the ($\alpha + \beta$) spin density is the charge density. The the α spin transfer $\simeq$ β spin transfer $\simeq$ 0.1 e, from chlorine to cobalt, in agreement with theory. However, the experimental spin density shows that the ($\alpha - \beta$) spin population is *not* the value of 0.03 given by the theory, but rather 0.08. It appears that the calculations are neglecting terms that affect the spin density more than the charge density. These terms may well be a free

$CoCl_4^{2-}$ ion problem, particularly electron correlation as indicated above. However, it is also possible that they are associated with the 'intermolecular' or 'crystal-field' polarisation effects noted, which affect the charge-density distributions within the $CoCl_4^{2-}$ ion, by as much as do the covalence effects. They also appear to give a better account of departures from cubic symmetry in the $CoCl_4^{2-}$ ion than do the positions of the chloride ions alone, as well as of the substantial observed polarisations of the chloride and caesium ions.

Acknowledgements

The authors are grateful to the Australian Research Grants scheme for financial support, to the Western Australian Regional Computing Centre for subsidised computing, and to the Crystallography Centre for data measurement.

References

1 B. N. Figgis, P. A. Reynolds, and S. Wright, *J. Am. Chem. Soc.*, 1983, **105**, 434.
2 B. N. Figgis, P. A. Reynolds, and R. Mason, *J. Am. Chem. Soc.*, 1983, **105**, 440.
3 G. S. Chandler, B. N. Figgis, R. A. Phillips, P. A. Reynolds, R. Mason, and G. A. Williams, *Proc. R. Soc. London, Ser. A*, 1982, **384**, 31.
4 G. S. Chandler and R. A. Phillips, *J. Chem. Soc., Faraday Trans. 2*, 1986, 573.
5 B. N. Figgis, P. A. Reynolds, and G. A. Williams, *J. Chem. Soc., Dalton Trans.*, 1980, 2339.
6 P. A. Reynolds, B. N. Figgis, and A. H. White, *Acta Crystallogr., Sect. B*, 1981, **37**, 508.
7 B. N. Figgis, P. A. Reynolds, and R. Mason, *Inorg. Chem.*, 1984, **23**, 1149.
8 B. N. Figgis, P. A. Reynolds, and A. H. White, *Inorg. Chem.*, 1985, **24**, 3762.
9 B. N. Figgis, P. A. Reynolds, and R. Mason, *Proc. R. Soc. London, Ser. A*, 1982, **384**, 49.
10 B. N. Figgis, P. A. Reynolds, and G. A. Williams, *J. Chem. Soc., Dalton Trans.*, 1980, 2348.
11 B. N. Figgis, J. B. Forsyth, R. Mason, and P. A. Reynolds, *Chem. Phys. Lett.*, 1985, **115**, 454.
12 B. N. Figgis and P. A. Reynolds, *Inorg. Chem.*, 1985, **24**, 1864.
13 H. Jorgensen, *Mol. Phys.*, in the press.
14 G. S. Chandler, R. Deeth, B. N. Figgis, K. Fujima, and M. I. Ogden, unpublished work.
15 M. A. Porai-Koshits, *Kristallografiya*, 1956, **1**, 291.
16 B. N. Figgis, M. Gerloch, and R. Mason, *Proc. R. Soc. London, Ser. A*, 1964, **279**, 210.
17 J. N. McElearney, S. Merchant, G. E. Shankle, and R. L. Carlin, *J. Chem. Phys.*, 1977, **66**, 450.
18 H. W. J. Blöte and W. J. Huiskamp, *Physica*, 1971, **53**, 445.
19 T. P. Melia and R. Merrifield, *J. Chem. Soc. A*, 1971, 1258.
20 J. Ferguson, *J. Chem. Phys.*, 1963, **39**, 116.
21 J. M. Stewart and S. R. Hall (eds.), 'The XTAL System of Crystallographic Programs: User's Manual,' Computer Science Technical Report TR-901, University of Maryland, 1983.
22 'International Tables for *X*-Ray Crystallography,' Kynoch Press, Birmingham, 1977, vol. 4, p. 102.
23 V. Schomaker and K. N. Trueblood, *Acta Crystallogr., Sect. B*, 1968, **24**, 63.
24 E. Clementi and C. Roetti, *At. Data Nucl. Data Tables*, 1974, **14**, 177.
25 R. Reschke, A Trautwein, F. E. Harris, and S. K. Date, *J. Magn. Magn. Mater.*, 1979, **12**, 176.
26 M. Miyake, H. Morikawa, and S. I. Iwai, *Acta Crystallogr., Sect. B*, 1980, **36**, 532.
27 J. Almlöf and J. Wahlgren, *Theor. Chim. Acta*, 1973, **28**, 161.
28 G. D. Mahan, *Chem. Phys. Lett.*, 1980, **76**, 183.
29 G. D. Mahan, *Phys. Rev. A*, 1980, **22**, 1780.
30 R. P. McEachran, A. D. Stauffer, and S. Greita, *J. Phys. B*, 1979, **12**, 3119.
31 P. J. Hay, *J. Chem. Phys.*, 1977, **66**, 4377.
32 D. P. Craig and E. A. Magnusson, *Discuss. Faraday Soc.*, 1958, **26**, 116.
33 P. Becker and P. Coppens, *Acta Crystallogr., Sect. A*, 1985, **41**, 177.

Received 19*th May* 1986; *Paper* 6/962